Applied Catalysis B: Environmental 201 (2017) 137–149

Contents lists available at ScienceDirect

Applied Catalysis B: Environmental

journal homepage: www.elsevier.com/locate/apcatb

Robust ruthenium catalysts for the selective conversion of stearic acid to diesel-range alkanes

Lu Di[a,1], Sikai Yao[a,1], Song Song[a], Guangjun Wu[a], Weili Dai[a], Naijia Guan[a,b], Landong Li[a,b,*]

[a] School of Materials Science and Engineering & National Institute for Advanced Materials, Nankai University, Tianjin 300071, PR China
[b] Key Laboratory of Advanced Energy Materials Chemistry of the Ministry of Education & Collaborative Innovation Center of Chemical Science and Engineering, Nankai University, Tianjin 300071, PR China

ARTICLE INFO

Article history:
Received 21 April 2016
Received in revised form 28 July 2016
Accepted 11 August 2016
Available online 12 August 2016

Keywords:
Ruthenium catalysts
Stearic acid
Catalytic deoxygenation
Biofuel
Reaction network

ABSTRACT

Triglycerides represent a type of sustainable energy source and robust catalysts for triglycerides refining to biofuels are very challenging. Herein, we report supported ruthenium catalysts, optimized from group VIII metal catalysts, for the selective conversion of triglycerides to diesel-range alkanes under mild conditions. The catalyst supports and ruthenium loadings show significant impacts on the performance of ruthenium catalysts, and Ru/TiO_2 with ruthenium weight loading of 1.68% is optimized for the reaction. Typically, the platform compound stearic acid could be directly converted, or via 1-octadecanol as an intermediate product, to *n*-heptadecane and *n*-octadecane in *n*-heptane solvent using the optimized Ru/TiO_2 catalyst at 473 K and under 3 MPa H_2. On the basis of catalytic and spectroscopic characterization results, large ruthenium metal particles are established as the preferred active sites for stearic acid conversion. The complete reaction network of stearic acid deoxygenation on flat Ru (0001) is investigated by theoretical calculations. It is revealed that different pathways run simultaneously during the reaction and the adsorbed acyl species $C_{17}H_{35}CO^*$ are the key reaction intermediates for the catalytic deoxygenation on Ru (0001). The removal of adsorbed CO by hydrogenation is the rate-controlling step contributing to the highest energy barrier within the reaction network.

1. Introduction

Nowadays, the diminishing fossil fuel reserves and the environmental problems caused by the excessive use of fossil fuels have triggered growing interest in alternative sustainable energy sources. Biomass, e.g. polysaccharides, lignin and triglycerides, is a very promising candidate with apparent advantages of abundance, low-cost and eco-friendliness [1–3]. Typically, triglycerides from natural oils or fats show great potential as a biomass energy source due to their extremely structural resemblance to diesel-type hydrocarbons [4–6]. Triglycerides can be selectively converted to applicable biofuels through refining processes with the reduction of their high oxygen content and related acidity.

Different strategies have been explored for the refining of triglycerides. Catalytic or enzymatic transesterification of triglycerides with methanol or ethanol, has been used commercially to product fatty acid alkyl esters, which can be viewed as the first-generation biodiesel [4,7–9]. Such alkyl esters, however, suffer from key disadvantages of high residual oxygen contents and high viscosities that limit their applications to some extent. Thermal cracking, also known as pyrolysis, of triglycerides represents an alternative strategy to derive biofuels [10,11]. While the loss of carbon and the decreasing energy content in products are inevitable, and the formation of aromatics and coke will further hinder the application of biofuels obtained. To overcome the drawbacks of transesterification and thermal cracking, the selective catalytic deoxygenation is developed. During the catalytic deoxygenation process, decarboxylation, decarbonylation and hydrodeoxygenation run simultaneously to efficiently remove the oxygen from the triglycerides and diesel-range alkanes are obtained as the final products. Under conventional hydrotreating conditions, standard hydrodesulfurization catalysts, e.g. sulphided nickel and molybdenum, are highly active in the conversion of triglycerides to

* Corresponding author at: School of Materials Science and Engineering & National Institute for Advanced Materials, Nankai University, Tianjin 300071, PR China.
E-mail address: lild@nankai.edu.cn (L. Li)
[1] These authors contributed equally to this work.

http://dx.doi.org/10.1016/j.apcatb.2016.08.023
0926-3373/

straight chain alkanes [12,13]. However, the sulfur leaching from sulphides could not only lead to the deactivation of catalysts but also result in the contamination of the alkane products. Supported noble metals have also been extensively investigated for the catalytic deoxygenation of triglycerides or their model compounds and palladium/carbon represent a very promising catalyst in semi-batch reactor test if its deactivation is not considered [14–16]. Recently, bifunctional catalysts based on nickel metal and acidic supports have been developed for the quantitative conversion of triglycerides to diesel-range diesels via cascade reactions, which show great potential for the production of green biofuels at large scale [17–19]. According to the existing studies on the catalytic deoxygenation of triglycerides, it is very clear that catalyst is the key issue for the whole refining process. Among all the catalysts investigated, 4%Pt-4%Re/TiO_2 was reported to exhibit remarkable catalytic activity in the conversion of fatty acid at very low temperature [20]. New catalysts are being explored [21,22], however, adequate catalysts working under mild conditions are still challenging. Typically, the catalytic deoxygenation of triglycerides or their model compounds is performed at ~573 K [23], making this process energy-consuming and expensive for operation. Moreover, the high temperature will complicate the reaction network and keep us from the understanding of individual steps in the deoxygenation reaction.

In the present study, robust ruthenium catalysts are developed for the catalytic deoxygenation of triglycerides to diesel-range alkanes and the reaction temperature is successfully lowered by ~100 K to below 473 K. The active ruthenium sites are identified and the detailed deoxygenation reaction network is established via the combination of experimental observations and theoretical calculations.

2. Experimental

2.1. Preparation of supported metal catalysts

Common materials, i.e. SiO_2 (Sinopec, surface area: 206 m^2/g), ZrO_2 (Alfa, surface area: 69 m^2/g), TiO_2 (Degussa P25, surface area: 51 m^2/g), CeO_2 (Acros, surface area: 51 m^2/g) and active carbon (Alfa, surface area: 249 m^2/g), were used as catalyst supports. Diffluent metal salts ($H_2PtCl_6{\cdot}xH_2O$, $PdCl_2$, $RuCl_3{\cdot}xH_2O$, $RhCl_3{\cdot}xH_2O$ and $H_2IrCl_6{\cdot}6H_2O$, all from Acros) were dissolved in distilled water to derive aqueous solutions with metal concentration of 1.0 mg/mL and then used as precursors for supported metals. The catalysts were prepared by impregnating the supports with aqueous solution of metal salts in a rotary evaporator at constant temperature. In a typical preparation process of Ru/TiO_2, 18 mL $RuCl_3$ aqueous solution was added to 1 g TiO_2 support. The impregnated sample was well mixed and then evaporated in a rotary evaporator at constant temperature of 353 K. The as-prepared sample was carefully washed by distilled water, dried at 353 K overnight, calcined in flowing dry air at 523 K for 1 h and then reduced in 5%H_2/He at 523 K for 1 h (Ru/C sample was reduced at 673 K) prior to being used as catalyst.

2.2. Characterization techniques

The exact metal loadings in supported catalysts were analyzed on an IRIS Advantage inductively coupled plasma atomic emission spectrometer (ICP-AES).

The specific surface areas of samples were determined through N_2 adsorption/desorption isotherms at 77 K collected on a Quantachrome iQ-MP gas adsorption analyzer.

The X-ray diffraction (XRD) patterns of TiO_2 samples were recorded on a Bruker D8 ADVANCE powder diffractometer using Cu-Kα radiation (λ = 0.1542 nm) at a scanning rate of 4°/min in the region of 2θ = 10–80°.

Transmission electron microscopy (TEM) images were taken on a FEI Tecnai G^2 F20 electron microscope at an acceleration voltage of 200 kV. A few drops of alcohol suspension containing the sample were placed on a carbon-coated copper grid, followed by evaporation at ambient temperature.

X-ray photoelectron spectra (XPS) of samples were recorded on a Kratos Axis Ultra DLD spectrometer with a monochromated Al-Kα X-ray source (hν= 1486.6 eV), hybrid (magnetic/electrostatic) optics and a multi-channel plate and delay line detector. All spectra were recorded by using an aperture slot of 300 × 700 μm. Accurate binding energies (±0.1 eV) were determined with respect to the position of the adventitious C 1 s peak at 284.8 eV.

The dispersion of metal on support was determined by CO pulse adsorption on a chemisorption analyzer (Chemisorb 2720, Micromeritics). In a typical experiment, *ca.*100 mg sample in the quartz reactor was first reduced in 5%H_2/He at 523 K for 1 h and purged with He at 523 K for 1 h to remove H_2 adsorbed on the surface of samples. After cooling down to room temperature in flowing He, pulses of 5%CO/He were injected to the reactor one pulse per minute until no further changes in signal intensity of outlet CO. The dispersion of metal was calculated assuming the equimolar adsorption of CO on metal.

The temperature-programmed reduction by hydrogen (H_2-TPR) experiments was carried out on a chemisorption analyzer (Quantachrome ChemBET 3000) with 5%H_2/Ar at a heating rate of 10 K/min from 300 to 1000 K. Prior to reduction, the sample (100 mg) was calcined in dry air at 523 K for 1 h.

FTIR spectra of CO adsorption on selected Ru/TiO_2 sample were collected on a Bruker Tensor 27 spectrometer with the resolution of 4 cm^{-1}. A self-supporting sample pellet was placed in the reaction chamber and the background spectrum was taken at 383 K in flowing He. After the He stream was switched to a gas mixture containing 1% CO in He, time-dependent FTIR spectra of CO adsorption Ru/TiO_2 were recorded at 383 K.

2.3. Catalytic evaluation and product analysis

The hydrodeoxygenation of stearic acid (Adamas, 99%) and its corresponding esters, i.e. methyl stearate (Adamas, 99%) and glycerol tristearate (Sigma, 99%), was performed in a high-pressure stainless autoclave (Xinyuan Chemical Machinery, Series CJK, 300 mL) at a stirring rate of 750 rpm. In a typical experiment, 0.2 g catalyst (micrometer-scale aggregates consisting of nano-scale particles; Fig. S1), 1 g stearic acid and 100 mL *n*-heptane solvent were well mixed in the autoclave and purged with pure N_2 at room temperature. The autoclave was heated to desired temperature (413–473 K) at a rate of 20 K/min and H_2 was then introduced at 3 MPa (total pressure, vapor pressure of *n*-heptane solvent at 413–473 K was 0.4-0.6 MPa) to initiate the reaction.

After reaction, the organic layer and aqueous layer were separated and the liquid organic products were analyzed by gas chromatography (Shimadzu GC-2010) and gas chromatography–mass spectrometry (Shimadzu GCMS-QP2010 SE), both with a RXI-5MS column (30 m, 0.25 mm i.d., stationary phase thickness 0.25 μm). *n*-Eicosane was used as an internal standard for quantification and carbon balance of >90% was obtained for all reactions. The following temperature program was employed: isothermal heating at 323 K for 5 min, heating to 573 K with a rate of 10 K/min, and isothermal heating at 573 K for 10 min. After reaction, the gas products were qualitatively analyzed with a mass spectrometer (Pfeiffer Omnistar GSD 320).

Table 1
Stearic acid hydrodeoxygenation over different catalysts.[a]

Catalyst	S_{BET} (m^2/g)	Metal wt.%	Dispersion (%)[b]	Conversion (%)	Alkanes Yield (%)	Product Selectivity (%)[c]			Reaction rate (mol/h mol_{Me})[c]	TOF (/h)[c]
						$C_{18}H_{37}OH$	$C_{18}H_{38}$	$C_{17}H_{36}$		
Ir/TiO_2	51	1.62	26.1	23.8	4.5	78.9	9.7	12.4	16.0	61
Pd/TiO_2	50	1.66	23.5	22.8	3.1	81.1	0	18.9	4.9	21
Pt/TiO_2	50	1.64	30.8	4.2	0	>99.9	0	0	3.2	10
Rh/TiO_2	50	1.87	33.9	65.7	32.9	59.8	5.0	35.2	19.2	57
Ru/TiO_2	50	1.68	28.2	96.3	32.7	78.2	3.7	18.1	34.1	120
Ru/ZrO_2	68	1.63	37.5	55.9	28.9	76.9	0.8	12.3	19.9	53
Ru/SiO_2	202	1.64	25.4	11.0	2.7	77.4	3.5	19.1	3.8	15
Ru/CeO_2	50	1.58	28.7	26.3	8.2	68.8	1.3	29.9	8.6	30
Ru/C	245	1.89	33.7	4.3	2.3	45.9	2.9	51.2	3.1	9
Pd/C	242	1.92	31.5	9.7	2.3	76.7	2.5	20.8	6.3	20
Ru/TiO_2	51	0.41	46.9	20.3	5.4	72.8	4.2	23.0	21.3	45
Ru/TiO_2	51	0.83	35.1	42.1	14.1	66.6	3.6	29.8	32.9	93
Ru/TiO_2	49	3.29	13.3	72.5	32.7	67.5	3.1	29.3	15.5	117
TiO_2	51	/	/	0	0	/	/	/	/	/

[a] Reaction conditions: 1.0 g stearic acid, 100 mL *n*-heptane, 0.2 g catalyst, 3 MPa H2, temperature = 473 K, time = 3 h.
[b] Measured by CO chemisorption.
[c] Value at low stearic acid conversion of ~10%.

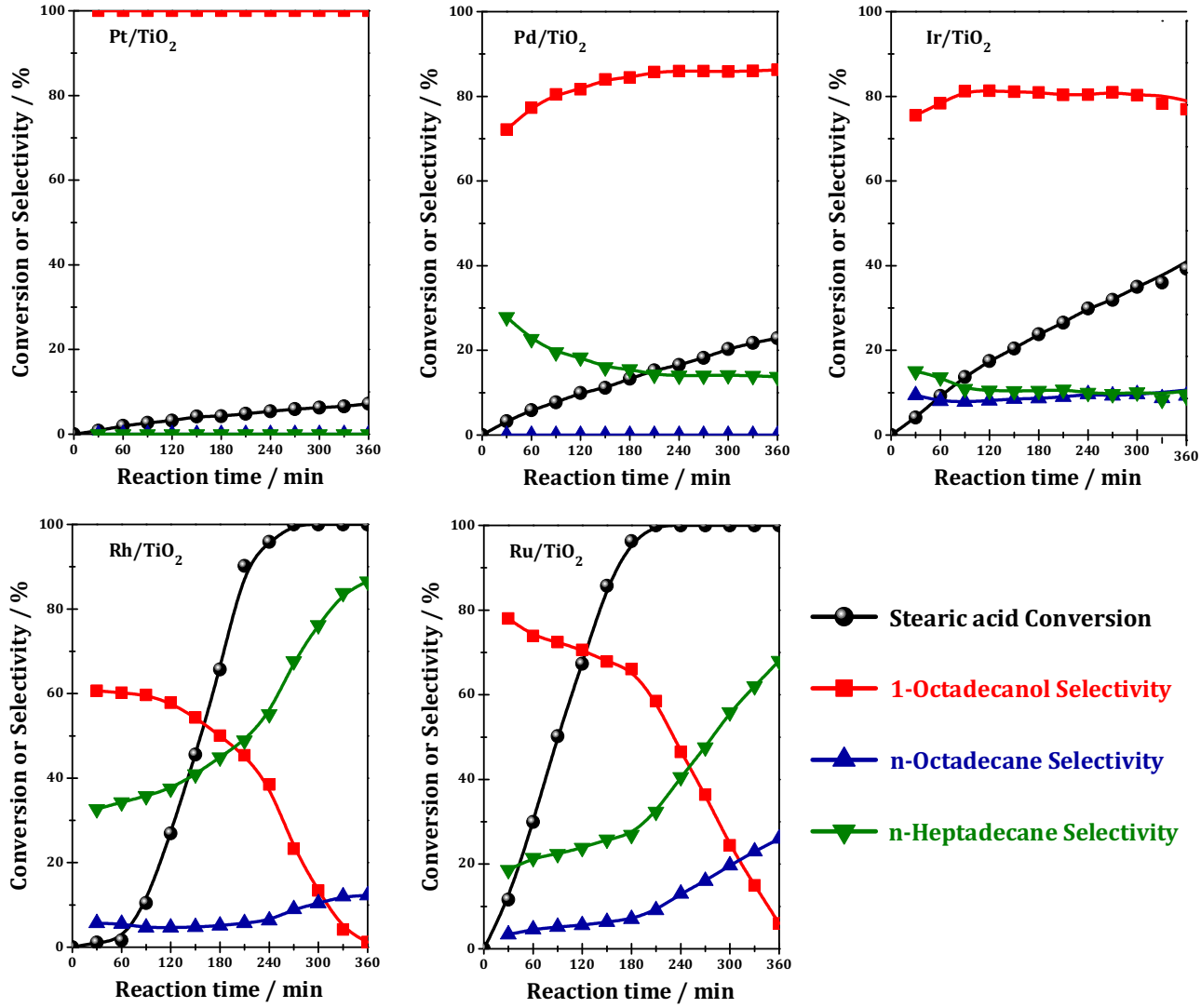

Fig. 1. Time-dependent behavior of stearic acid conversion over TiO_2 supported catalysts. Reaction conditions: 1.0 g stearic acid, 100 mL *n*-heptane, 0.2 g catalyst, 3 MPa H_2, temperature = 473 K.

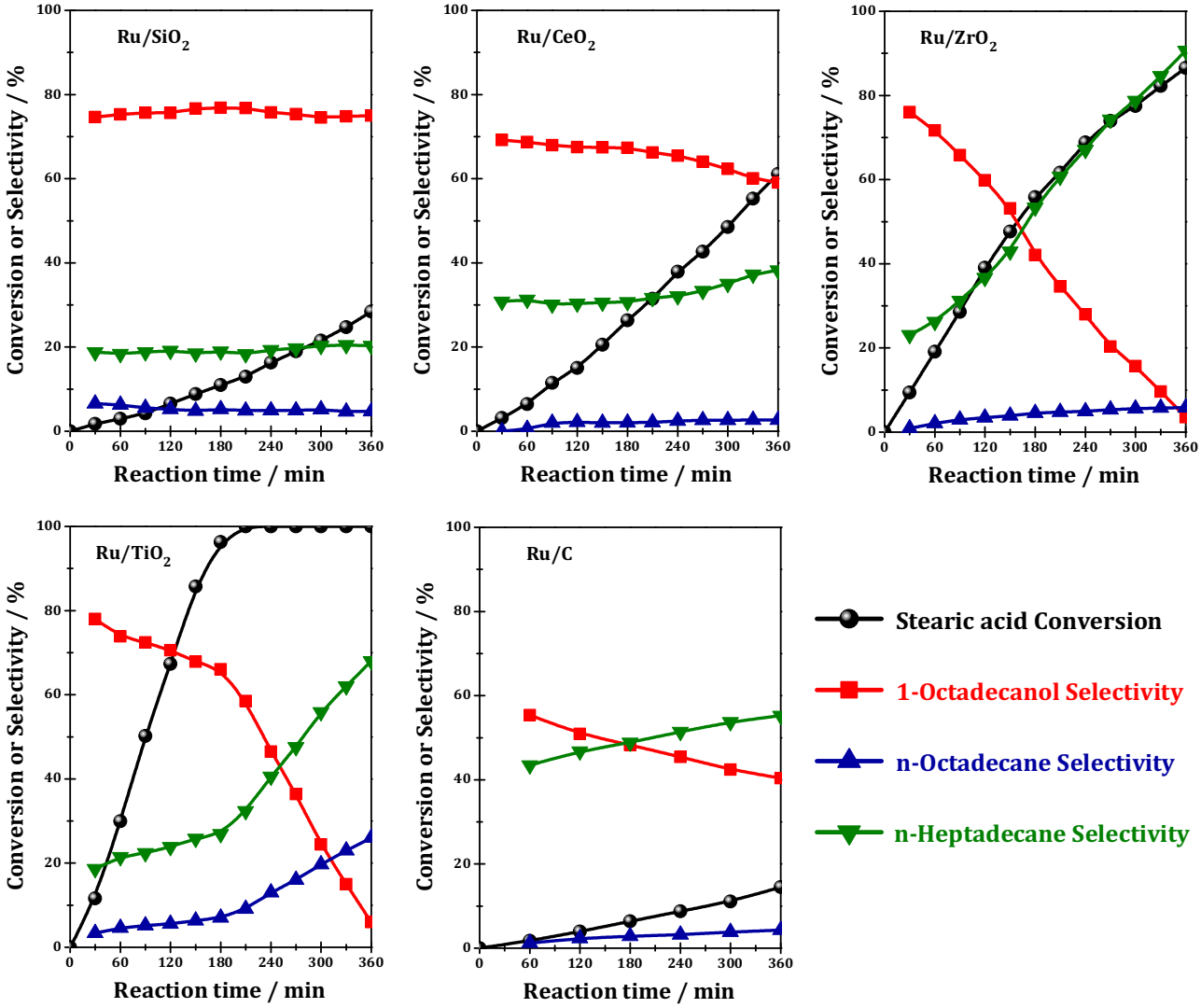

Fig. 2. Time-dependent behavior of stearic acid conversion over supported ruthenium catalysts. Reaction conditions: 1.0 g stearic acid, 100 mL *n*-heptane, 0.2 g catalyst, 3 MPa H_2, temperature = 473 K.

2.4. Calculation methods and models

The activation barriers, total energy changes with and without pre-adsorbed atomic oxygen and the corresponding analysis were performed by self-consistent periodical density functional theory (DFT) calculations using the Vienna ab initio simulation package (VASP) [24,25]. The electronic structures were calculated using DFT within GGA-PW91 functional [26]. The projector augmented wave (PAW) Scheme [27,28] was used to describe the inner cores, and the electronic states were expended in a plane wave basis with kinetic cut-off energy of 400 eV. The transition states (TS) were located by three steps: the general NEB method [29,30] was employed to find an approximated TS, then the quasi-Newton algorithm was used to optimize the likely TSs until the force acting on the atom is smaller than 0.03 eV/Å, and last the frequency analysis was carried out to confirm the TS. Ru (0001) is modeled by the p (8*4) unit cell of three layers that are separated by a ~15 Å in vacuum. The optimized lattice constant is 2.75 Å. Since the relative large unit cell was used in this study, only one Γ-point was used to sample the first Brillouin zone [31]. The adsorption energy E_{ads} (at surface coverage of 1/20 ML for stearic acid and 1-octadecanol considering the steric-hindrance effects from bulky molecules, and 1/4 ML for CO and H_2) is calculated by the formula $E_{ads} = E_{mix} - E_{slab} - E_{gas}$, where E_{mix}, E_{slab}, and E_{gas} indicate the calculated energy of the ruthenium slab with an adsorbate binding onto it, clean slab, and adsorbate in the gas phase, respectively.

3. Results and discussion

3.1. Screening of catalysts and exploring of active sites

A series of supported group VIII noble metal catalysts were tested in the deoxygenation of stearic acid as a model reaction under mild conditions, e.g. at 473 K and under 3 MPa H_2. As shown in Table 1, TiO_2 supported group VIII noble metals exhibited quite different catalytic behavior in the reaction. Low stearic acid conversion rates were obtained with Pt/TiO_2 (3.2 mol/h mol_{Me}) and Pd/TiO_2 (4.9 mol/h mol_{Me}), while the highest stearic acid conversion rate of 34.1 mol/h mol_{Me} was obtained with Ru/TiO_2. The kinetic behavior of stearic acid conversion over Ru/TiO_2 and Rh/TiO_2 (Fig. 1) reveals that the product distributions change with reaction time, indicating that different reaction steps run simultaneously during the reaction. After reaction for 6 h, diesel-range alkanes, i.e. *n*-heptadecane and *n*-octadecane, were obtained as

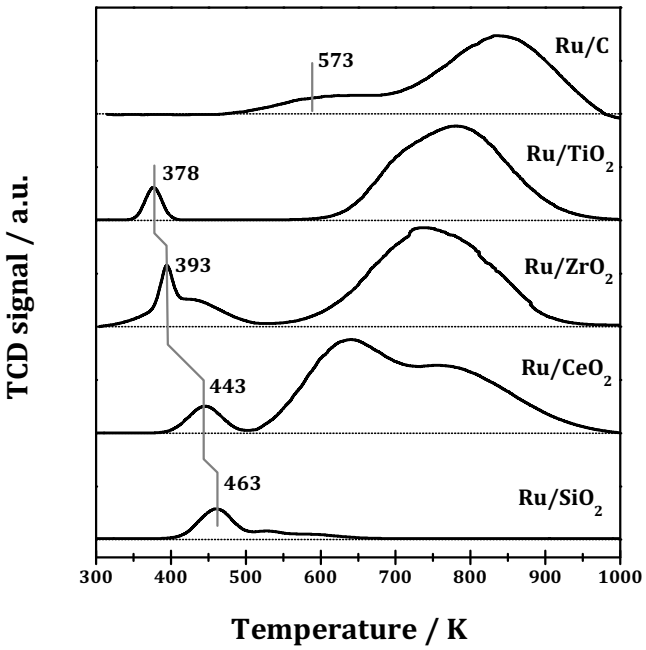

Fig. 3. H_2-TPR profiles of supported ruthenium catalysts.

dominating products from stearic acid conversion over Ru/TiO_2 and Rh/TiO_2 (>95%), which appear to be the adequate deoxygenation catalysts working under mild conditions. Ru/TiO_2 should be more attracting one due to the much lower price of ruthenium than rhodium.

The effects of support materials on the stearic acid conversion over ruthenium catalysts were further investigated. As shown in Table 1 & Fig. 2, ruthenium catalysts on different supports (XRD patterns shown in Fig. S1) exhibited different conversion rates of stearic acid and the product distributions in the reaction. TiO_2 appears to be the best support employed, followed by ZrO_2 and then CeO_2 and SiO_2. It is interesting to note that commonly-used Ru/C catalyst exhibited very low activity under our reaction conditions. If the reaction temperature was increased to 553 K, the catalytic activity of Ru/C (Fig. S2) could be greatly enhanced to the level even higher than literature reports (Here, the preparation and pretreatment conditions will greatly influence the catalytic activity of Ru/C) [15,24].

Ru 3d XP spectra of unreduced supported ruthenium catalysts (Fig. S3) indicate that ruthenium species exist in the similar cationic states on different supports before reduction treatment. The existing states of ruthenium species on different supports were further investigated by means of H_2-TPR and the results are shown in Fig. 3. Since the oxide supports are almost irreducible below 500 K, the reduction peaks in the temperature range of 300–500 K should come from the reduction of cationic ruthenium species. Unsupported ruthenium oxides are known to give a hydrogen reduction peak at around 373 K [32], and the existence of support materials will generally retard the reduction of cationic ruthenium species due to the metal-support interaction. In this study, the reducibility of ruthenium species on different supports is observed as $Ru/TiO_2 > Ru/ZrO_2 > Ru/CeO_2 > Ru/SiO_2$, correlating well with the catalytic activity of supported ruthenium catalysts. It is known that the catalytic activity of supported ruthenium catalysts can be affected by many factors including the ruthenium metal size, distribution and metal-support interaction. Meanwhile, the reducibility of ruthenium species are affected by these factors. Thereupon, the reducibility of ruthenium species are relevant with the catalytic activity. According to the H_2-TPR results, ruthenium species on oxide supports could be reduced to the metallic form below 523 K and metallic ruthenium species should dominate in the working catalysts that were pre-reduced at 523 K for 1 h. FTIR spectra of CO adsorption (Fig. S4) further confirm that ruthenium metals are the only detectable ruthenium species in Ru/TiO_2 after reduction. For Ru/TiO_2, the reduction of cationic ruthenium species occurs at ~378 K, much lower than the reaction temperature of 473 K employed. That is, cationic ruthenium species could be reduced and kept at metallic states during the reaction process with high pressure of pure hydrogen. In fact, both un-reduced Ru/TiO_2 (Fig. S5) and pre-reduced Ru/TiO_2 (Fig. 2) exhibit similar good activity in the catalytic deoxygenation of stearic acid. On the basis of above-mentioned experimental results, it is reasonable to propose that metallic ruthenium species are the active sites for the catalytic deoxygenation of stearic acid.

Fig. 3 Ruthenium loadings show distinct impacts on the performance of Ru/TiO_2 catalysts in the conversion of stearic acid. As shown in Fig. 4, the stearic acid conversion rate first increases with ruthenium loading from 0.41 to 1.68% and then decreases with ruthenium loading further increase to 3.29%. While the percentage of alkanes, i.e. *n*-octadecane and *n*-heptadecane, in the product distribution keeps increasing with ruthenium loading from 0.41 to 3.29%. TEM observations (Fig. 5) reveal that the ruthenium particle size on TiO_2 support gradually increases from <1 to ~5 nm with increasing ruthenium loading and the size-dependent ruthenium catalyzed stearic acid conversion could be drawn, as shown in Fig. 6. The initial TOF value increases distinctly with increasing ruthenium particle size on TiO_2 and reaches a plateau at the ruthenium size of ~2.5 nm, indicating that large ruthenium metal particles are more active for stearic acid conversion. For practical consideration, 1.68% is the optimized ruthenium loading and $1.68\%Ru/TiO_2$ will be employed as a model catalyst in the following sections. For $1.68\%Ru/TiO_2$ catalyst, the average ruthenium particle size is 2.6 nm (Fig. 5), meaning that one ruthenium particle contains about 800 ruthenium atoms. Under such circumstances, flat Ru (0001) is the dominating surface in Ru/TiO2 and, therefore, selected as a model for theoretical calculation.

3.2. Temperature and solvent effects on stearic acid deoxygenation

Reaction temperature shows significant impacts on the deoxygenation of stearic acid over Ru/TiO_2 catalyst. As expected, the conversion rate increases with increasing reaction temperature from 413 to 473 K (Fig. 7). 1-Octadecanol, *n*-octadecane and *n*-heptadecane were obtained as products in the liquid phase and methane as an exclusive product in the gas phase in the whole temperature range studied. Time-dependent product yields from stearic acid conversion (Fig. S6) show that the yield of individual product increases linearly with time before the total conversion of stearic acid, indicating that parallel reaction steps run simultaneously to generate different products. The pseudo-zero order reactions observed here also indicate the limited active sites for stearic acid conversion, which should be associated with the steric hindrance effects from the bulky reactants. The time-dependent 1-octadecanol yields during stearic acid conversion at different temperatures over Ru/TiO_2 are drawn in Fig. 8. It is clearly seen that 1-octadecanol is produced linearly with time from stearic acid deoxygenation. After the total conversion of stearic acid, 1-octadecanol is further converted to *n*-octadecane and *n*-heptadecane, leading to the linear decrease with time in the 1-octadecanol yield. This should be explained from the competitive adsorption between 1-octadecanol and stearic acid on the active ruthenium sites. Calculation results indicate that the adsorption of stearic acid (adsorption energy: −0.66 eV) is much stronger than 1-octadecanol (adsorption energy: −0.50 eV) on Ru (0001). That

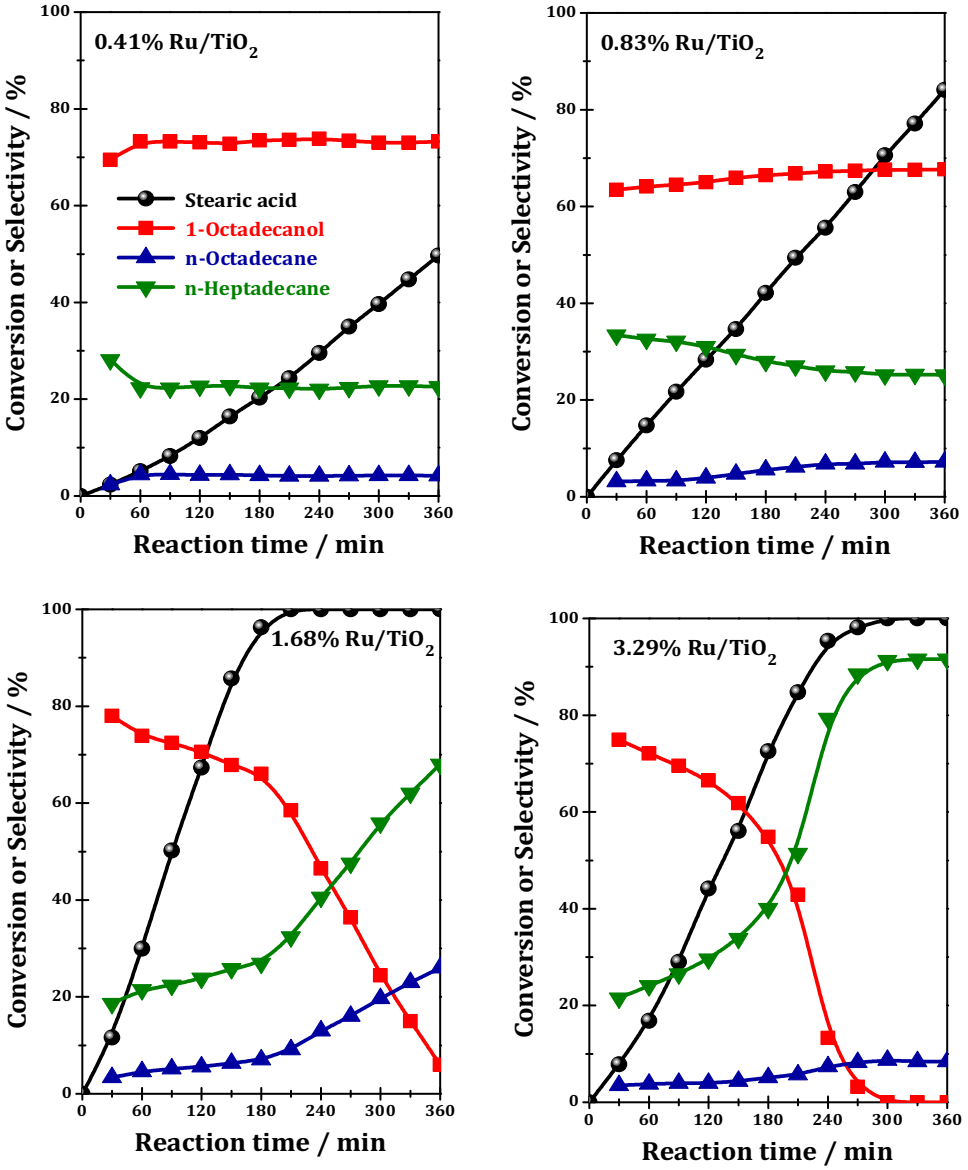

Fig. 4. Time-dependent behavior of stearic acid conversion over Ru/TiO_2 with different ruthenium loadings. Reaction conditions: 1.0 g stearic acid, 100 mL *n*-heptane, 0.2 g catalyst, 3 MPa H_2, temperature = 473 K.

is, the existence of stearic acid in the reaction system will hinder the further conversion of product 1-octadecanol by preferentially occupying the active ruthenium sites. Arrhenius plots (Fig. 9) reveal that the apparent activation energy of stearic acid conversion to 1-octadecanol over Ru/TiO_2 is 62.4 kJ/mol, distinctly lower than the subsequent 1-octadecanol conversion to alkanes (94.5 kJ/mol).

3.3. Recycling test and triglycerides conversion

The stability of catalyst is very important for practical biomass conversion. In this study, the recyclability of Ru/TiO_2 catalyst in the catalytic deoxygenation of stearic acid is tested and the results are shown in Fig. 10. A gradual loss of catalytic activity for the conversion of stearic acid to alkanes could be observed for Ru/TiO_2 and the yield of total alkane yield after 6 h reaction decreases from 95 to 45% after three recycles. No ruthenium species could be detected in the organic phase even after reaction for 6 h (below the ICP detection limit of 20 ppb), excluding the leach of ruthenium species during the reaction. Since the general means for coke analysis, e.g. temperature-programmed oxidation and thermogravimetric analysis, could not be applied for catalyst samples employed in solid-liquid reaction system, the possible formation of coke on the surface of catalyst could not be verified. However, the chance for coke formation in hydrogenation reaction is not very high. In such circumstance, we propose that the loss of catalytic activity in Ru/TiO_2 should originate from the reconstruction of ruthenium sites during reaction, i.e. the re-dispersion of ruthenium species induced by interacting with reactant and/or products [33,34]. Fortunately, the activity of Ru/TiO_2 can be fully recovered after a regeneration step, i.e. calcination at 573 K in air for 1 h followed by reduction in hydrogen at 523 K for 1 h, and the total alkane yield of 96% could be obtained with regenerated catalyst after 6 h reaction (initial TOF value of 112 h^{-1}). Representative TEM images of Ru/TiO_2 sample after three recycling tests and after calcination-reduction treatment are shown in Fig. 11. It is observed that the average ruthenium particle size on TiO_2 decreases from 2.7 nm to 2.1 nm after three recycling tests, while it increases to 4.5 nm after calcination-reduction treatment. These experimental results

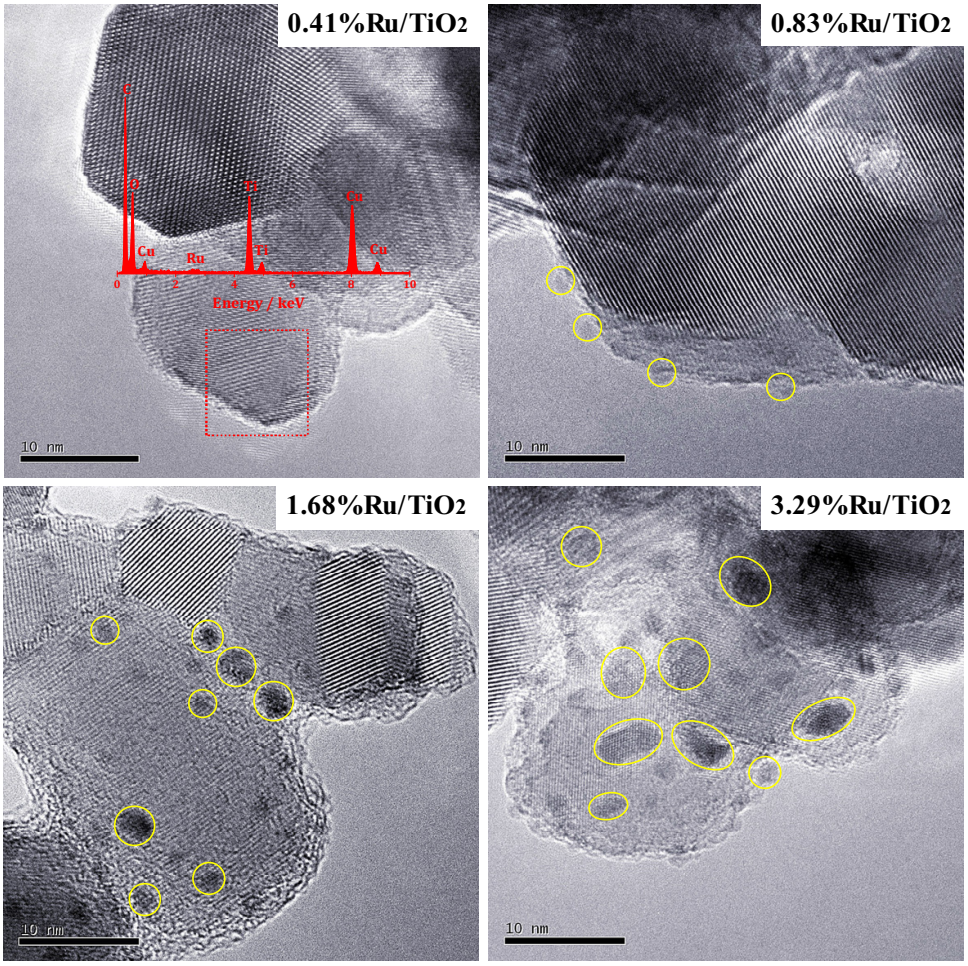

Fig. 5. TEM images of Ru/TiO_2 samples with different ruthenium loadings.

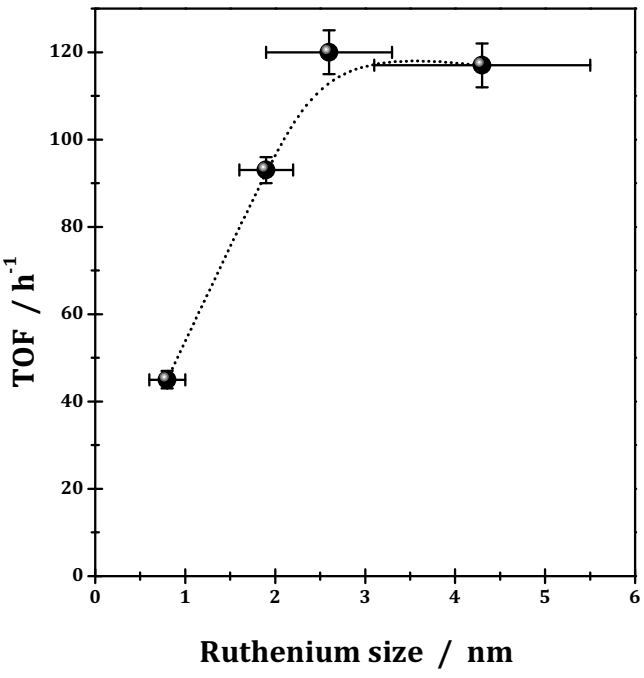

Fig. 6. Comparison of initial TOF values in stearic acid conversion catalyzed by Ru/TiO_2 with different ruthenium sizes.

confirm our previous conclusion that the initial TOF value reaches a plateau at the ruthenium size of ~2.5 nm.

With the great success of Ru/TiO_2 in the catalytic deoxygenation of stearic acid as a platform compound, we further investigate the catalytic behavior of Ru/TiO_2 in the deoxygenation of methyl stearate and glycerol tristearate. As shown in Fig. 12, Ru/TiO_2 exhibit very good performance in these two reactions under mild conditions and alkanes could be obtained as final products. Typically, methyl stearate and glycerol tristearate can be fullly converted to diesel-range alkanes after reaction for 4 and 12 h, respectively. The much lower conversion rate of glycerol tristearate as compared to methyl stearate should be due to the significant steric-hindrance effect from reactant molecule that may block a large part of available ruthenium sites for the catalytic deoxygenation. It should be mentioned that gaseous product from methyl stearate conversion is methane, similar to the conversion of stearic acid (Fig. S8). While for the conversion of glycerol tristearate, both propane and methane can be detected as gaseous products (Fig. S8). These results clearly indicate the hydrogenolysis of ester bonds as the first step for the deoxygenation of aliphatic esters.

3.4. Modeling of stearic acid deoxygenation on flat Ru (0001)

Fig. 13 Extensive experimental and theoretical investigations have been conducted on the hydrogenolysis of carboxylic acids to alcohols and the further conversion of alcohols to alkanes [35–41]. It was proposed that carboxylic acids could dissociate to form the acyl intermediates, which undergo hydrogenation to alcohols. The

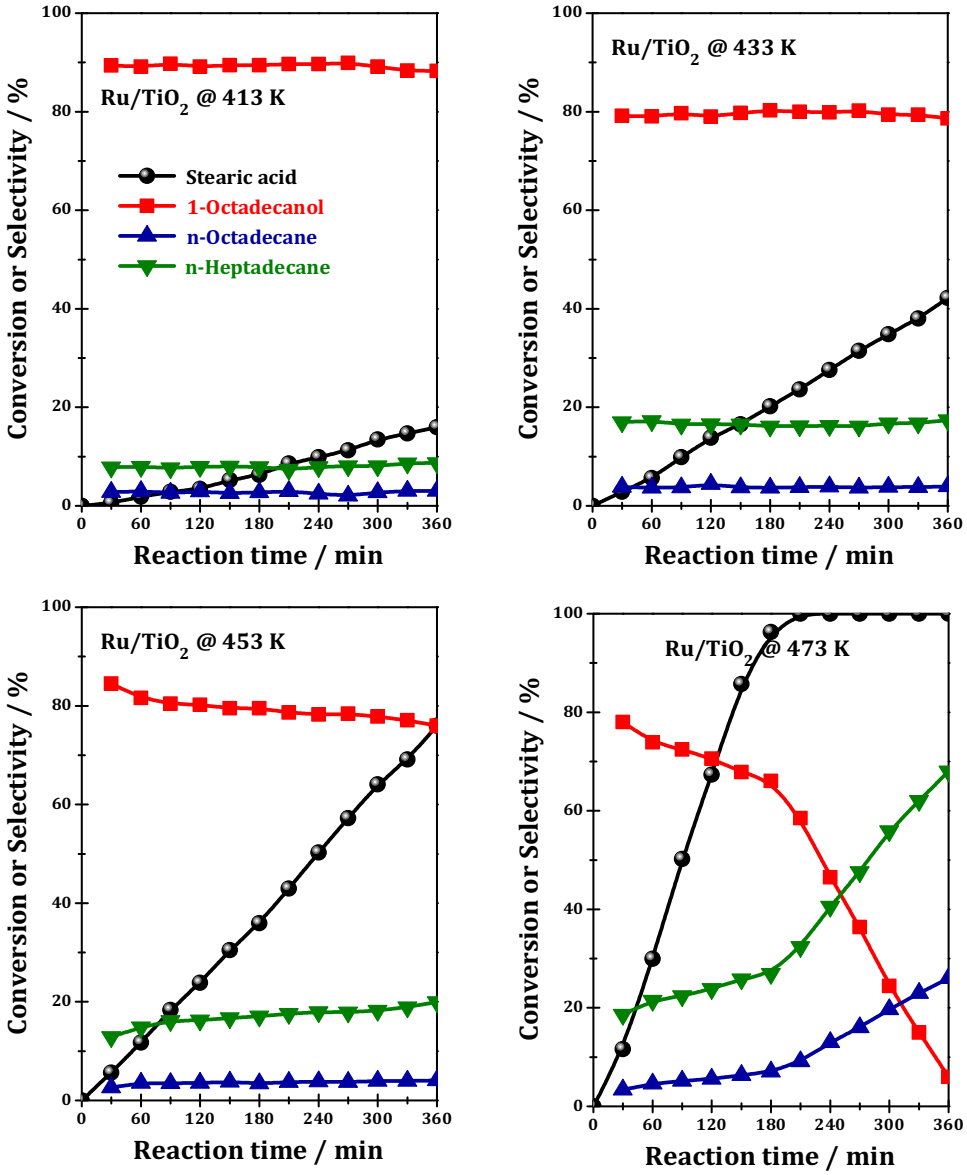

Fig. 7. Time-dependent behavior of stearic acid conversion over 1.68%Ru/TiO_2 catalyst. Reaction conditions: 1.0 g stearic acid, 100 mL *n*-heptane, 0.2 g catalyst, 3 MPa H_2, temperature = 413–473 K.

acyl intermediates could also be activated via the cleavage of β-C—H bond, and then undergo the scission of C—C or C—O bonds to yield alkanes.

On the basis of our experiment results, four pathways may run simultaneously during the catalytic deoxygenation of stearic acid, i.e. (i) stearic acid conversion to 1-octadecanol, (ii) stearic acid conversion to alkanes, (iii) 1-octadecanolconversion to alkanes, and (iv) CO hydrogenation to methane. DFT calculations were performed on Ru (0001) to give an insight of the complete reaction network in stearic acid deoxygenation. The complete reaction network is illustrated in Fig. 13 (transition state configurations shown in Fig. S9) and the individual reaction step is summarized in Table 2.

The adsorption and hydrodeoxygenation of stearic acid is the beginning of the reaction. Stearic acid that absorbs on the surface of Ru (0001) through oxygen and hydrogen undergoes a dehydroxylation with a low energy barrier of 0.44 eV, generating the acyl intermediate $C_{17}H_{35}CO^*$. The acyl intermediate $C_{17}H_{35}CO^*$ will further undergo hydrogenation to 1-octadecanol and hydrodeoxygenation to alkanes. Calculation results indicate that both pathways have very similar energy barrier for the rate-controlling steps (1.28 and 1.20 eV, Table 2) and the barriers are low enough for reaction under conditions employed in this study (vide infra). According to our experimental observations (Fig. 2), 1-octadecanol is the dominating product at the early stage of reaction, which should be explained from the different kinetic behavior of competing reactions. The apparent formation rates of 1-octadecanol, *n*-heptadecane and *n*-octadecane at 473 K are calculated (from experiments) to be 0.85, 0.28 and 0.07 μmol/h, respectively.

The hydrogenation of the acyl intermediate $C_{17}H_{35}CO^*$ may undergo two possible paths, and adding hydrogen atom to carbon atom of $C_{17}H_{35}CO$ is energy favored (0.63 eV) over that to oxygen atom (1.19 eV). Hydrogen atom could add to carbon and then oxygen atom of $C_{17}H_{35}CHO$ species, leading to the formation of 1-octadecanol product. Adding hydrogen to carbon atom of $C_{17}H_{35}CHO$ species is an exothermic reaction with an energy barrier of 0.69 eV and the subsequent hydrogenation of $C_{17}H_{35}CH_2O$ bears a high energy barrier 1.28 eV. Alternatively, hydrogen could add to oxygen atom of $C_{17}H_{35}CHO$ to generate $C_{17}H_{35}CHOH$ species

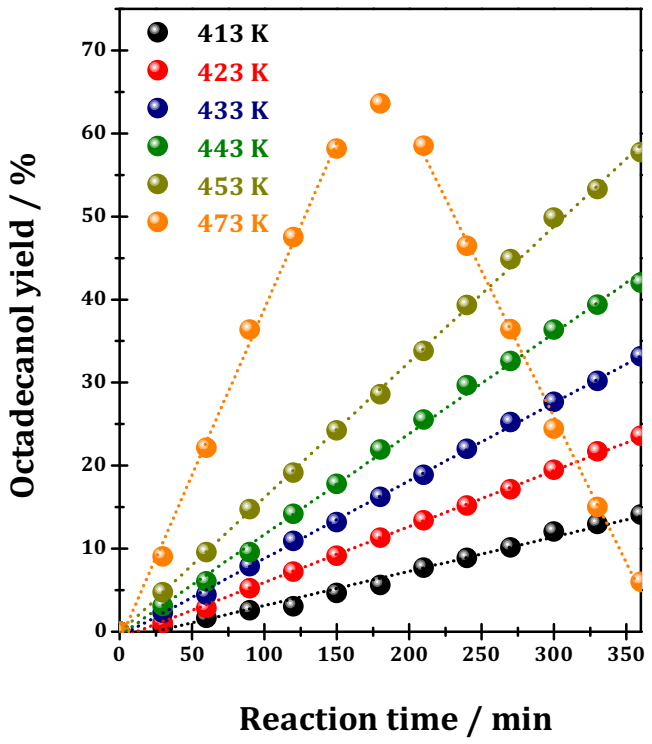

Fig. 8. Time-dependent 1-octadecanol yields during stearic acid conversion over 1.68%Ru/TiO_2 catalyst. Reaction conditions: 1.0 g stearic acid, 100 mL *n*-heptane, 0.2 g catalyst, 3 MPa H_2, temperature = 413–473 K.

(1.20 eV), which is less energetically favored than the formation of $C_{17}H_{35}CH_2O$. However, the formed $C_{17}H_{35}CHOH$ species can undergo an exothermic hydrogenation reaction to generate 1-octadecanol with a low energy barrier of 0.87 eV, which is the most likely pathway from the acyl intermediate to 1-octadecanol.

The acyl intermediate $C_{17}H_{35}CO^*$ could also undergo the β-carbon-hydrogen bond activation to produce $C_{16}H_{33}CHCO$ species with low energy barrier of 0.53 eV. The $C_{16}H_{33}CHCO$ species would be further converted to $C_{16}H_{33}CHC$ species via carbon-oxygen bond scission (1.21 eV) or to $C_{16}H_{33}CH$ species via carbon–carbon bond scission (1.08 eV). The cleavage of carbon–carbon bond is energetically preferred over that of carbon-oxygen bond, consistent with literature reports [42]. The oxygen-free $C_{16}H_{33}CHC$ and $C_{16}H_{33}CH$ species could then be hydrogenated to alkanes: $C_{16}H_{33}CH$ species take two successive hydrogenation steps to product $C_{14}H_{29}CH_3$ and $C_{16}H_{33}CHC$ species take four steps of hydrogenation to generate $C_{18}H_{38}$ via the route of $C_{14}H_{29}CHC \rightarrow C_{14}H_{29}CHCH \rightarrow C_{14}H_{29}CH_2CH \rightarrow C_{14}H_{29}CH_2CH_2 \rightarrow C_{14}H_{29}CH_2CH_3$. All hydrogenation steps are easy to occur with energy barriers below 0.8 eV.

The intermediate product 1-octadecanol could undergo hydrogenolysis to generate alkanes. Since the desorption energy of stearic acid (0.66 eV) is much higher than that of 1-octadecanol (0.50 eV), 1-octadecanol could not adsorb on ruthenium surface in the presence of unconverted stearic acid in the reaction system, as confirmed in our experiments (Fig. 8) and also in agreement with literature reports on ReO_x/TiO_2 catalyst [43]. After the complete conversion of stearic acid, 1-octadecanol begins to adsorb on ruthenium surface through oxygen atom and undergoes the cleavage of oxygen-hydrogen bond with a lowest energy barrier of 0.72 eV compared with the cleavage of α-carbon-hydrogen, β-carbon-hydrogen, oxygen-hydrogen, carbon–carbon and carbon–oxygen bond [44]. The product $C_{17}H_{35}CH_2O$ species then undergo two steps of α-carbon-hydrogen bond cleavage (0.88 and 0.28 eV) to produce the $C_{16}H_{33}CH_2CO$ species, i.e. the

Table 2
Calculated reaction energies (ΔH), energy barriers (Ea), and bond lengths of transition states (d) on flat Ru (0001) surface.

Entry	Reaction step	ΔH (eV)	Ea (eV)	d (Å)
01	$RCH_2COOH + * \rightarrow RCH_2COOH^*$	−0.66	/	/
02	$RCH_2COOH^* \rightarrow RCH_2CO^* + OH^*$	−0.12	0.44	1.92
03	$RCH_2CO^* + H^* \rightarrow RCH_2CHO^*$	0.35	0.63	1.19
04	$RCH_2CO^* + H^* \rightarrow RCH_2COH^*$	0.70	1.19	1.42
05	$RCH_2CHO^* + H^* \rightarrow RCH_2CH_2O^*$	−0.19	0.69	1.56
06	$RCH_2CHO^* + H^* \rightarrow RCH_2CHOH^*$	0.48	1.20	1.41
07	$RCH_2COH^* + H^* \rightarrow RCH_2CHOH^*$	0.10	0.54	1.38
08	$RCH_2CH_2O^* + H^* \rightarrow RCH_2CH_2OH^*$	0.56	1.28	1.40
09	$RCH_2CHOH^* + H^* \rightarrow RCH_2CH_2OH^*$	−0.16	0.87	1.51
10	$RCH_2CH_2OH + * \rightarrow RCH_2CH_2OH^*$	−0.50	/	/
11	$RCH_2CH_2OH^* \rightarrow RCH_2CH_2O^* + H^*$	−0.56	0.72	1.40
12	$RCH_2CH_2O^* \rightarrow RCH_2CHO^* + H^*$	0.19	0.88	1.56
13	$RCH_2CHO^* \rightarrow RCH_2CO^* + H^*$	−0.35	0.28	1.19
14	$RCH_2CO^* \rightarrow RCHCO^* + H^*$	−0.12	0.53	1.57
15	$RCHCO^* \rightarrow RCHC^* + O^*$	−0.37	1.20	1.88
16	$RCHCO^* \rightarrow RCH^* + CO^*$	−0.41	1.08	2.02
17	$RCH^* + H^* \rightarrow RCH_2^*$	0.39	0.72	1.67
18	$RCH_2^* + H^* \rightarrow RCH_3$	−0.20	0.67	1.62
19	$RCHC^* + H^* \rightarrow RCHCH^*$	0.20	0.47	1.64
20	$RCHCH^* + H^* \rightarrow RCH_2CH^*$	0.24	0.52	1.64
21	$RCH_2CH^* + H^* \rightarrow RCH_2CH_2^*$	0.39	0.72	1.67
22	$RCH_2CH_2^* + H^* \rightarrow RCH_2CH_3$	−0.20	0.67	1.62
23	$CO^* \rightarrow C^* + O^*$	0.42	>2	/
24	$CO^* \rightarrow CO + *$	1.98	/	/
25	$CO^* + H^* \rightarrow HCO^*$	1.04	1.29	1.14
26	$HCO^* + H^* \rightarrow H_2CO^*$	0.39	0.31	1.52
27	$H_2CO^* \rightarrow CH_2^* + O^*$	−0.68	0.78	2.01
28	$CH_2^* + H^* \rightarrow CH_3^*$	0.06	0.55	1.64
29	$CH_3^* + H^* \rightarrow CH_4$	−0.18	0.67	1.57
30	$H_2 + * \rightarrow H_2^*$	−0.49	/	/
31	$H_2^* + * \rightarrow 2H^*$	−0.46	/	/
32	$O^* + H^* \rightarrow OH^* + *$	0.48	0.95	1.26
33	$OH^* + H^* \rightarrow H_2O^*$	0.10	0.91	1.50
34	$H_2O^* \rightarrow H_2O + *$	0.40	/	/

acyl intermediate. Once the acyl intermediate is formed, it could be further converted to $C_{14}H_{29}CH_3$ and $C_{14}H_{29}CH_2CH_3$, sharing the partial route of stearic acid to alkanes.

CO, the byproduct from carbon–carbon bond scission of $C_{16}H_{33}CHCO$ species, strongly adsorbs on ruthenium surface with a highest desorption energy among all reactants and products, and, therefore, it has a huge inhibition impact on the whole reaction. Considering that clean surface is required for the adsorption and conversion of stearic acid, the adsorbed CO must be removed from Ru (0001) to trigger the reaction. Calculation results suggest that adsorbed CO species prefer to undergoing hydrogenation to CH_4 with a barrier of 1.29 eV rather than the dissociation into C* and O* with a barrier of >2 eV or the direct desorption with 1.98 eV, which agrees well with experimental observation of CH_4 as the dominating gaseous product (Fig. S8). A feasible hydrogenation pathway is established as $CO^* \rightarrow HCO^* \rightarrow H_2CO^* \rightarrow CH_2^* \rightarrow CH_3^* \rightarrow CH_4$. The first step $CO^* \rightarrow HCO^*$ is the rate-controlling step with the highest energy barrier, similar to previous reports on Rh (111) [45]. CO hydrogenation to CH_4 is thermodynamically favored due to the fact that the reaction is highly exothermic. In fact, CO hydrogenation ($CO^* + H^* \rightarrow HCO^*$) contributes to the highest energy barrier within the complete reaction network of stearic acid deoxygenation. During the whole reaction process, the formed *O species on clean Ru (0001) surface readily react with *H to produce H_2O (*O + *H → * + *OH; $OH^* + H^* \rightarrow H2O^*$; Table 2). Therefore, Ru (0001) should be kept in the metallic state during the reaction in the excess of high pressure hydrogen.

Fig. 14 As mentioned above, parallel reaction steps run simultaneously during the deoxygenation of stearic acid over ruthenium catalysts. The reactant stearic acid can be directly converted to 1-octadecanol and alkanes via competing pathways. After the complete conversion of stearic acid, the intermediate product

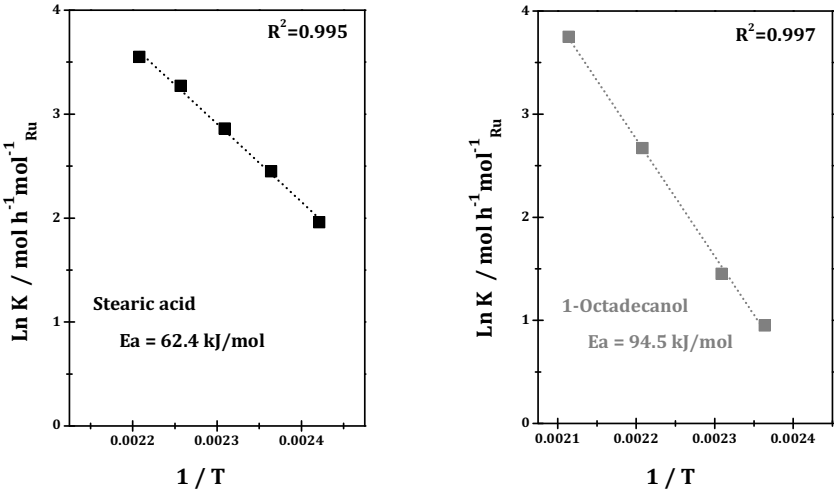

Fig. 9. Arrhenius plots of stearic acid conversion to 1-octadecanol and subsequent 1-octadecanol to alkanes catalyzed by Ru/TiO_2.

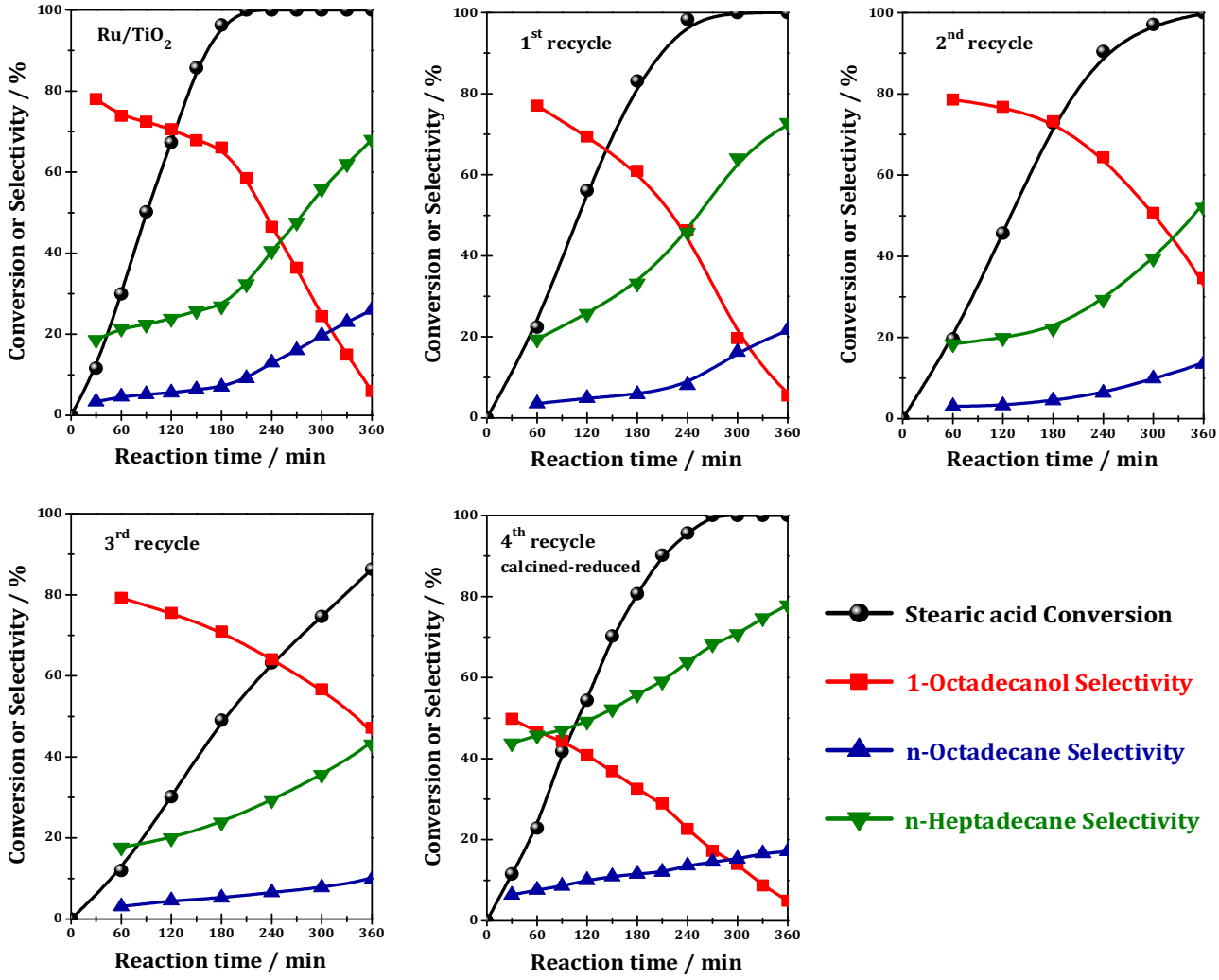

Fig. 10. Catalyst recycling studies of stearic acid conversion over 1.68%Ru/TiO_2 catalyst. Reaction conditions: 1.0 g stearic acid, 100 mL *n*-heptane, 0.2 g catalyst, 3 MPa H_2, temperature = 473 K.

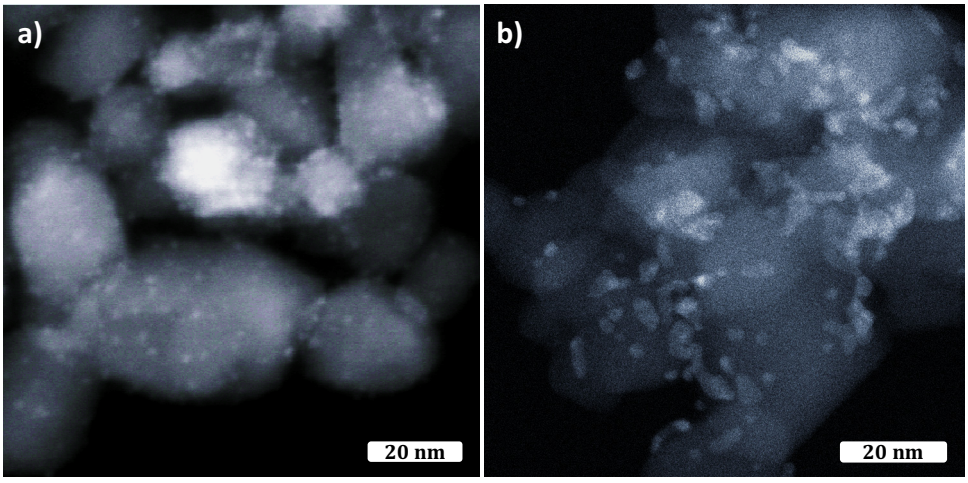

Fig. 11. HAADF-STEM images of Ru/TiO_2 after three recycling tests of stearic acid conversion for 6 h (a) and after calcination-reduction post-treatment (b).

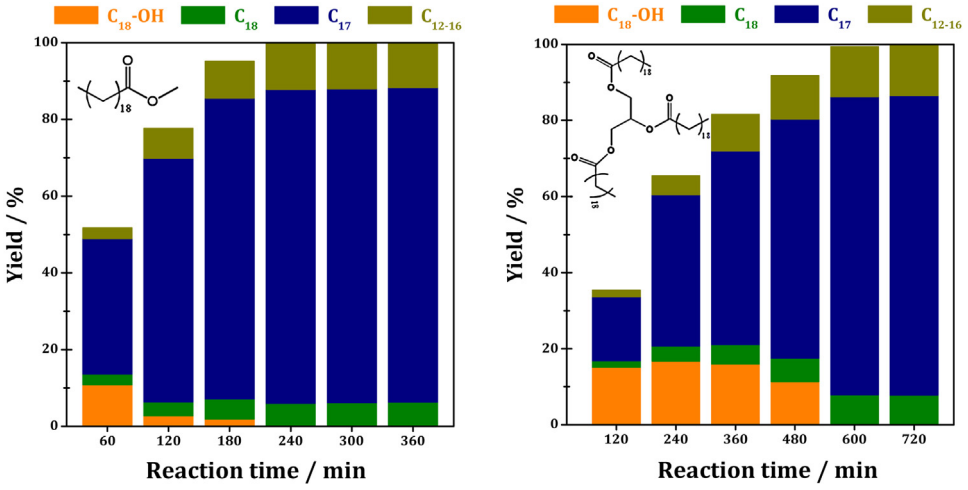

Fig. 12. Time-dependent behavior of methyl stearate and glycerol tristearate conversion over 1.68%Ru/TiO_2 catalyst. Reaction conditions: 1.0 g methyl stearate or glycerol tristearate, 100 mL *n*-heptane, 0.2 g catalyst, 3 MPa H_2, temperature = 473 K; Stearate and glycerol tristearate dissolve well in *n*-heptane.

1-octadecanol can also be converted to alkanes. The adsorbed acyl $C_{17}H_{35}CO^*$ is established as a key reaction intermediate in the deoxygenation network. The removal of adsorbed CO from carbon–carbon bond scission of $C_{16}H_{33}CHCO$ species is the rate-controlling step contributing to the highest energy barrier within the complete reaction network. The calculated energy profile of stearic acid conversion is summarized in Fig. 14. On the basis of theoretical calculations results, it can be proposed that Ru (0001) surface is eligible to catalyze the conversion of stearic acid to alkanes by its self and the dominating role of support is carry the active metal sites. Besides, modifications on ruthenium sites to promote the removal of adsorbed CO species should be an effective means to improve the activity of ruthenium catalysts.

4. Conclusions

In summary, supported ruthenium materials are presented as robust catalysts for the selective conversion of triglycerides to diesel-range alkanes under mild conditions. The platform compound stearic acid could be converted to 1-octadecanol, *n*-heptadecane and *n*-octadecane with optimized Ru/TiO_2 catalyst at low temperature of 473 K, while 1-octadecanol could be further converted to *n*-heptadecane and *n*-octadecane after the complete conversion of stearic acid under identical reaction conditions. The ruthenium species in Ru/TiO_2 should exist in the metallic form during reaction and large ruthenium metal particles with weak metal-support interaction are established as the preferred active sites for stearic acid conversion. A gradual loss of catalytic activity in stearic acid conversion is observed for Ru/TiO_2 in recycling tests, however, the catalytic activity could be fully recovered after a simple calcination-reduction treatment, which is very important for practical biomass refining.

Theoretical calculations reveal that parallel reaction steps run simultaneously during the conversion of stearic acid deoxygenation on flat Ru (0001), and the complete reaction network is successfully constructed. The adsorbed acyl species $C_{17}H_{35}CO^*$ are key reaction intermediates for the catalytic deoxygenation of stearic acid, while the removal of adsorbed CO, i.e. by-product from carbon–carbon bond scission of $C_{16}H_{33}CHCO$ species, is the rate-controlling step contributing to the highest energy barrier within the complete reaction network.

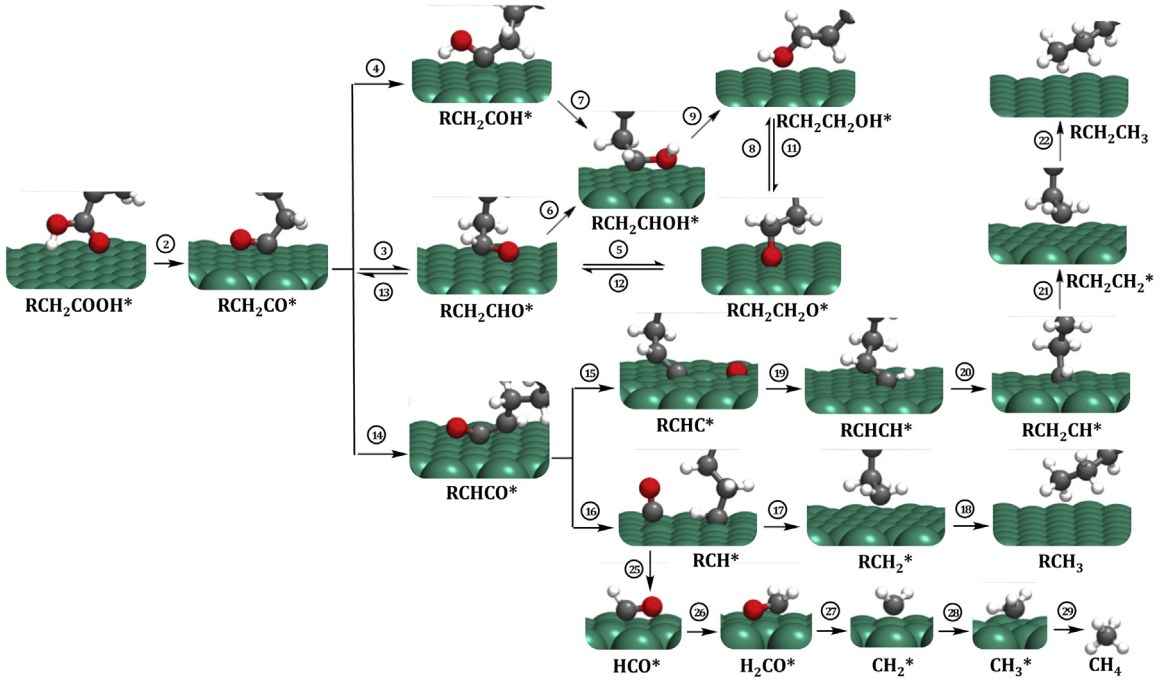

Fig. 13. Reaction network for the deoxygenation of stearic acid on flat Ru (0001). Individual reaction step labelled in accord with Entry in Table 2.

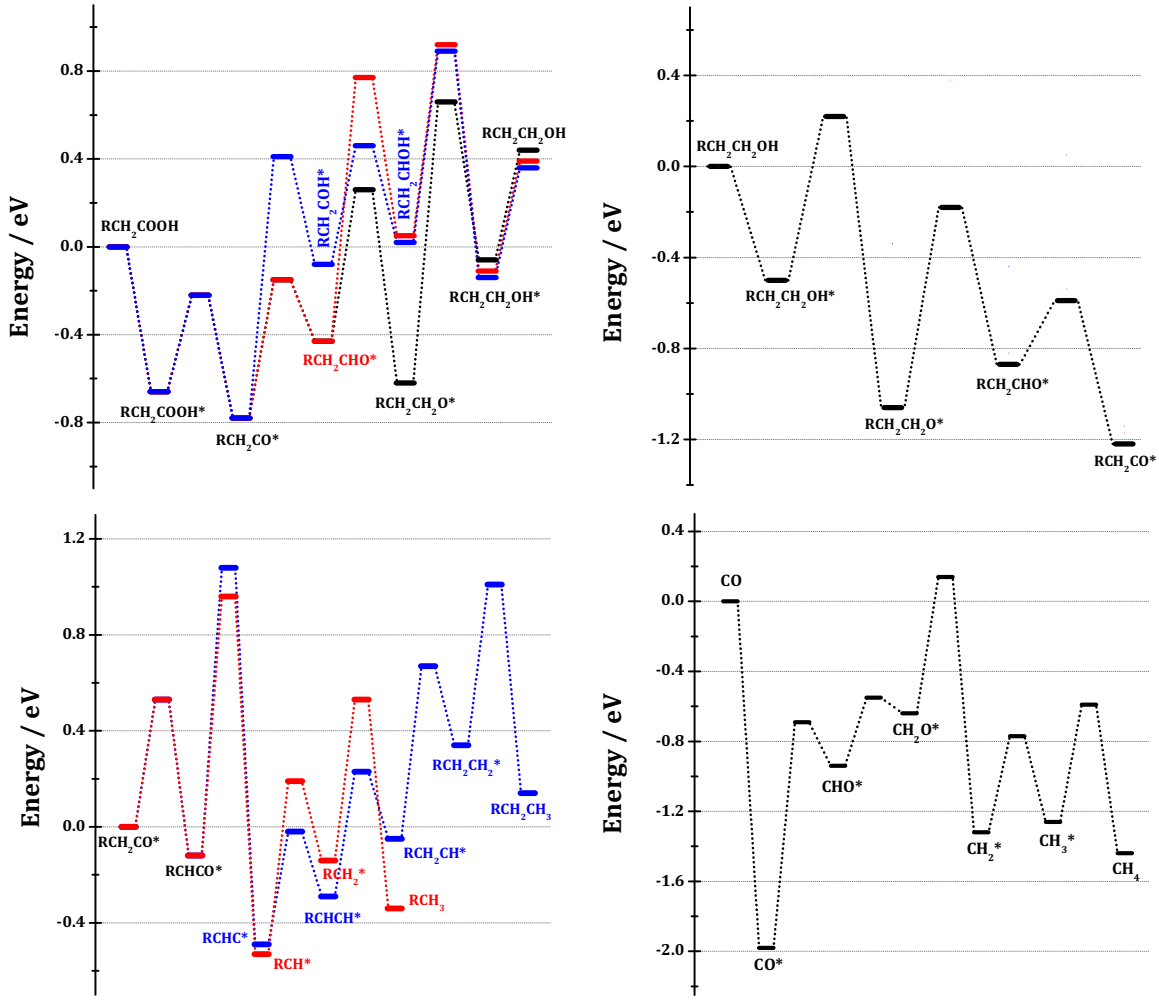

Fig. 14. Calculated energy profile for the deoxygenation of stearic acid on flat Ru (0001).

Acknowledgements

This work is supported by the National Natural Science Foundation of China (21421001, 21303087), Municipal Natural Science Foundation of Tianjin (13RCGFGX01124, 13JCQNJC05900), the Ministry of Education of China (IRT13022) and the 111 project (B12015).

Appendix A. Supplementary data

Supplementary data associated with this article can be found, in the online version, at http://dx.doi.org/10.1016/j.apcatb.2016.08.023.

References

[1] G.W. Huber, S. Iborra, A. Corma, Chem. Rev 106 (2006) 4044–4098.
[2] A. Corma, S. Iborra, A. Velty, Chem. Rev 107 (2007) 2411–2502.
[3] D.M. Alonso, J.Q. Bond, J.A. Dumesic, Green Chem. 12 (2010) 1493–1513.
[4] F. Ma, M.A. Hanna, Bioresour. Technol. 70 (1999) 1–15.
[5] Y. Chisti, Biotechnol. Adv. 25 (2007) 294–306.
[6] S. Lestari, P. Mäki-Arvela, J. Beltramini, G.Q. Max Lu, D.Y. Murzin, ChemSusChem 2 (2009) 1109–1119.
[7] H. Fukuda, A. Kondo, H. Noda, J. Biosci. Bioeng. 92 (2001) 405–416.
[8] E. Lotero, Y. Liu, D.E. Lopez, K. Suwannakarn, D.A. Bruce, J.G. Goodwin, Ind. Eng. Chem. Res. 44 (2005) 5353–5363.
[9] L.C. Meher, D. Vidya Sagar, S.N. Naik, Renew. Sustain. Energy Rev. 10 (2006) 248–268.
[10] A.W. Schwab, G.J. Dykstra, E. Selke, S.C. Sorenson, E.H. Pryde, J. Am. Oil Chem. Soc. 65 (1988) 1781–1786.
[11] K.D. Maher, D.C. Bressler, Bioresour. Technol. 98 (2007) 2351–2368.
[12] B. Donnis, R.G. Egeberg, P. Blom, K.G. Knudsen, Top. Catal. 52 (2009) 229–240.
[13] D. Kubička, L. Kaluža, Appl. Catal. A 372 (2010) 199–208.
[14] I. Kubičková, M. Snåre, K. Eränen, P. Mäki-Arvela, D.Y. Murzin, Catal. Today 106 (2005) 197–200.
[15] M. Snåre, I. Kubičková, P. Mäki-Arvela, K. Eränen, D.Y. Murzin, Ind. Eng. Chem. Res. 45 (2006) 5708–5715.
[16] M. Snåre, I. Kubičková, P. Mäki-Arvel, D. Chichova, K. Eränen, D.Y. Murzin, Fuel 87 (2008) 933–945.
[17] B. Peng, Y. Yao, C. Zhao, J.A. Lercher, Angew. Chem. Int. Ed. 51 (2012) 2072–2075.
[18] W. Song, C. Zhao, J.A. Lercher, Chem. Eur. J. 19 (2013) 9833–9842.
[19] B. Peng, X. Yuan, C. Zhao, J.A. Lercher, J. Am. Chem. Soc. 134 (2012) 9400–9405.
[20] H.G. Manyar, C. Paun, R. Pilus, D.W. Rooney, J.M. Thompsona, C. Hardacre, Chem. Commun. 46 (2010) 6279–6281.
[21] Y. Yang, C. O-Hernaíndez, V.A. O'shea, J.M. Coronado, D.P. Serrano, ACS Catal. 2 (2012) 592–598.
[22] R.W. Gosselink, D.R. Stellwagen, J.H. Bitter, Angew. Chem. Int. Ed. 52 (2013) 5089–5092.
[23] C. Zhao, T. Brück, J.A. Lercher, Green Chem. 15 (2013) 1720–1739.
[24] G. Kresse, J. Furthmüller, Comput. Mater. Sci. 6 (1996) 15–50.
[25] G. Kresse, J. Furthmuller, Phys. Rev. B 54 (1996) 11169–11181.
[26] J.P. Perdew, Y. Wang, Phys. Rev. B 45 (1992) 13244–13249.
[27] P.E. Blöchl, Phys. Rev. B 50 (1994) 17953–17979.
[28] G. Kresse, D. Joubert, Phys. Rev. B 59 (1999) 1758–1775.
[29] G. Mills, H. Jonsson, Phys. Rev. Lett. 72 (1994) 1124–1127.
[30] G. Henkelman, B.P. Uberuaga, H. Jonsson, J. Chem. Phys. 113 (2000) 9901–9904.
[31] H.J. Monkhorst, J.D. Pack, Phys. Rev. B 13 (1976) 5188–5192.
[32] L. Li, L. Qu, J. Cheng, J. Li, Z. Hao, Appl. Catal. B 88 (2009) 224–231.
[33] W.C. Ketchie, E.P. Maris, R.J. Davis, Chem. Mater. 19 (2007) 3406–3411.
[34] A.M. Abdel-Mageed, S. Eckle, R.J. Behm, J. Am. Chem. Soc. 137 (2015) 8672–8675.
[35] J. Lu, M. Faheem, S. Behtash, A. Heyden, J. Catal. 324 (2015) 14–24.
[36] R. Alcalá, M. Mavrikakis, J.A. Dumesic, J. Catal. 218 (2003) 178–190.
[37] V. Pallassana, M. Neurock, J. Catal. 209 (2002) 289–305.
[38] R. Shekhar, M.A. Barteau, R.V. Plank, J.M. Vohs, J. Phys. Chem. B 101 (1997) 7939–7951.
[39] M. Mavrikakis, M.A. Barteau, J. Mol. Catal. A 131 (1998) 135–147.
[40] R.D. Cortright, R.R. Davda, J.A. Dumesic, Nature 418 (2002) 964–967.
[41] L. Chen, Y. Zhu, H. Zheng, C. Zhang, B. Zhang, Y. Li, J. Mol. Catal. A 351 (2011) 217–227.
[42] E.I. Gürbüz, D.D. Hibbitts, E. Iglesia, J. Am. Chem. Soc. 137 (2015) 11984–11995.
[43] B. Rozmysłowicz, A. Kirilin, A. Aho, H. Manyar, C. Hardacre, J. Wärnå, T. Salmi, D.Y. Murzin, J. Catal. 328 (2015) 197–207.
[44] L. Di, S. Yao, M. Li, G. Wu, W. Dai, G. Wang, L. Li, N. Guan, ACS Catal. 5 (2015) 7199–7207.
[45] Y. Choi, P. Liu, J. Am. Chem. Soc. 131 (2009) 13054–13061.